JOURNAL OF SYNCHROTRON RADIATION
ISSN 1600-5775

Local atomic structure analysis around Mg atom doped in GaN by X-ray absorption spectroscopy and spectrum simulations

Noritake Isomura* and Yasuji Kimoto

Toyota Central R&D Laboratories Inc., 41-1 Yokomichi, Nagakute, Aichi 480-1192, Japan.
*Correspondence e-mail: isomura@mosk.tytlabs.co.jp

Received 1 February 2021
Accepted 14 April 2021

Edited by S. M. Heald, Argonne National Laboratory, USA

Keywords: X-ray absorption fine structure; density functional theory; magnesium; dopants; gallium nitride.

The identification of the incorporated site of magnesium (Mg) and hydrogen (H) required for p-type formation in gallium nitride (GaN) power devices has been demonstrated by X-ray absorption spectroscopy (XAS). In this study, the fluorescence line of Mg with 3×10^{19} atoms cm^{-3} was successfully separated from that of Ga using a superconducting tunnel junction array detector with high sensitivity and high energy resolution, and consequently the Mg *K*-edge XAS spectra of such dilute samples were obtained. The site of Mg atoms incorporated into the GaN lattice was identified as the Ga substitutional site by comparing the experimental XAS spectrum with the simulated spectra calculated by density functional theory. In addition, the presence or absence of H around Mg can be determined through distinctive characteristics expected from the spectrum simulations.

1. Introduction

Gallium nitride (GaN) has gained attention as a component of wide bandgap semiconductors for next-generation power devices (Kachi, 2014). However, controlling the conduction type of GaN has still been a significant challenge, especially in the case of p-type formation (Narita *et al.*, 2017). Typically, the p-type formation is conducted by introducing magnesium (Mg) as a dopant into GaN (Kanechika *et al.*, 2007), where Mg substitutes Ga sites in a lattice (Neugebauer & Walle, 1999). However, not all the doped Mg atoms are activated as acceptors. There are two possible reasons for this: (1) the doped Mg atoms are located at the Ga sites due to clustering (Bennett *et al.*, 2011) or (2) magnesium–hydrogen (Mg–H) complexes are formed which causes acceptor compensation (Nakamura *et al.*, 1992). In order to solve this problem, it is necessary to identify the Mg site and to analyze the existence of H around Mg atoms. However, the analytical methods for detecting H are limited and it is more difficult to identify its atomic site.

X-ray absorption spectroscopy (XAS) is a technique used to obtain information on the atomic structure about an element of interest (Norman, 1986). In XAS, partial fluorescence yield (PFY), which uses an energy-dispersive detector to acquire X-rays from only the target element, is advantageous for the detection of dilute elements because it can lower the background. By applying this technique to the analysis of Mg in GaN, one would think that it is possible to identify the Mg site and the surrounding atomic structure. However, in the case of a small amount of Mg contained in GaN, a large peak of Ga *L* lines is close to the peak of the Mg *Kα* line in X-ray fluorescence spectra; hence, it is difficult to obtain a spectrum of only

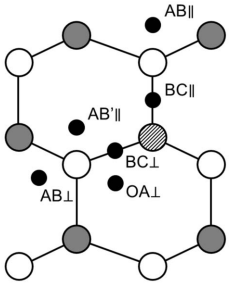

Mg using conventional detectors such as silicon drift detectors (SDDs) (Yonemura *et al.*, 2013). Therefore, a detector with high sensitivity and high energy resolution is required for the analysis of Mg-doped GaN. The National Institute of Advanced Industrial Science and Technology (AIST), Japan, has developed a superconducting tunnel junction (STJ) array detector with an energy resolution ten times higher than that of SDDs and a detection efficiency of several hundred times that of a wavelength-dispersive X-ray spectrometer (WDX) (Ohkubo *et al.*, 2012; Shiki *et al.*, 2014). The STJ array detector can allow the detection of a small amount of Mg contained in GaN. The atomic site of the target element cannot be identified only with the measured spectrum. Mizoguchi *et al.* (2009) conducted a systematic theoretical study using density functional theory (DFT) and reported that simulated spectra corresponded with the measured spectra in the spectral shape in X-ray absorption near-edge structure (XANES). Furthermore, we have also studied the incorporated atoms in semiconductors such as silicon carbide and gallium oxide, and showed the advantage of this combined experimental and theoretical technique (Isomura, Kutsuki *et al.*, 2019; Isomura, Kataoka *et al.*, 2019; Isomura *et al.*, 2020).

In this study, we demonstrated local atomic structure analysis around Mg doped in GaN by PFY-XAS measurements using the STJ array detector and XANES spectrum simulations using DFT. The Mg which substitutes the Ga site required for p-type formation was identified when the measured XANES spectrum was compared with the simulated spectra. In addition, the difference in spectra with H (compensating acceptors) was examined to clarify whether or not the presence or absence of H around Mg could be determined.

2. Experimental and theoretical methods

The sample used was an Mg-doped GaN film grown on a GaN (0001) substrate using a metal organic vapor-phase epitaxy method (Amano *et al.*, 1989), and it was subsequently annealed at 800°C for 5 min in nitrogen (N_2) to remove H. This is known as activation annealing. The film thickness and Mg concentration were 1 µm and 3×10^{19} atoms cm^{-3}, respectively, as measured using secondary ion mass spectrometry (SIMS).

The XAS measurements were performed at the undulator beamline BL-16A of the Photon Factory, Institute of Materials Structure Science, High Energy Accelerator Organization, Japan (Amemiya *et al.*, 2010). The beamline consists of a prefocusing mirror, an entrance slit and a varied-line-spacing plane grating monochromator, which provides linearly polarized soft X-rays in the energy range 200–1500 eV. The photon flux is $\sim 1 \times 10$ photons s^{-1}. The beam size at the sample position is less than 1 mm × 1 mm (horizontal × vertical). The fluorescence X-rays emitted from the sample surface are detected by the STJ array detector. The apparatus includes a 0.3 K cryostat, a cold finger for mounting a detector chip, field-effect-transistor-based charge-sensitive preamplifiers and a digital signal processing system with field programmable gate array chips for 160 pixels (Ohkubo *et al.*, 2012; Shiki *et al.*, 2014). The maximum counting rate is more than 1 million counts s^{-1}. The average energy resolution of the 160 pixels is ∼10 eV. The incidence and detection angles relative to the sample surface were both 45°. For the integrated intensity in the range 1225–1275 eV centered on the Mg *Kα* peak, the energy of the incident X-ray is swept to obtain the Mg *K*-edge XANES spectrum.

In the theoretical simulations, Mg-doped GaN was modeled by incorporating an Mg atom into the lattice. The total number of Ga and N atoms in each unit cell was 127. An H atom was additionally incorporated at six sites in the Mg-doped GaN model (Park & Chang, 2012), *i.e.* antibonding (AB), bond-centered (BC), and off-axis antibonding (OA) sites with two types of orientation each, parallel (∥) or perpendicular (⊥) to the *c* axis, as shown in Fig. 1. Geometry optimizations of the structures and XANES spectrum simulations were performed through DFT calculations using the *CASTEP* plane-wave code (Clark *et al.*, 2005), aided by software from *Materials Studio* (BIOVIA). The calculations were completed in the Perdew–Burke–Ernzerhof generalized gradient approximations using ultrasoft pseudopotentials (Perdew *et al.*, 1996). In the XANES calculations, the ultrasoft pseudopotentials were generated on the fly (Gao *et al.*, 2009), where one core hole was created in the 1*s* core level. The convergence parameters were set as follows: an energy tolerance of 5×10^{-6} eV atom^{-1}, a maximum displacement tolerance of 5×10^{-4} Å and a Monkhorst–Pack *k*-point mesh of $2 \times 2 \times 2$ for the Brillouin zone integration. The cutoff energies were 380 eV and 400 eV in the geometrical optimizations and the XANES spectra simulations, respectively. To make the computational XANES results comparable with the experimental results, the energy was broadened using an instrumental smearing of 0.5 eV. Transition energy cannot be estimated directly in the pseudopotential method. Therefore, it was derived from the total energy difference between the excited and ground states in accordance with the procedure established by Mizoguchi *et al.* (2009). However, the transition energy is overestimated by ∼1% relative to the absolute

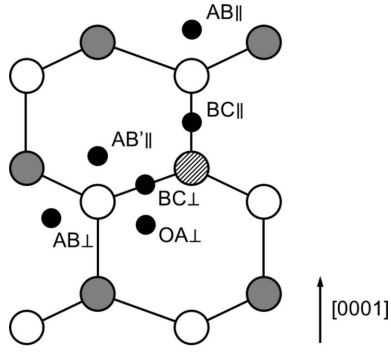

Figure 1
A schematic of the atomic sites for interstitial H in GaN (Park & Chang, 2012). Gray circles represent Ga atoms, white circles represent N atoms, the patterned circle represents an Mg atom and black circles represent H atoms. AB, BC and OA indicate antibonding, bond-centered and off-axis antibonding sites, respectively. These sites have two types of orientation: parallel (∥) or perpendicular (⊥) to the *c* axis.

energy (Mizoguchi *et al.*, 2012). Therefore, in this study, the energy of the simulated spectra was calibrated by determining the energy difference of the absorption edge (9 eV) from both calculated and experimental spectra obtained using $Mg(OH)_2$ as a common reference.

3. Results and discussion

The X-ray fluorescence spectrum for Mg-doped GaN irradiated with X-rays of 1350 eV is shown in Fig. 2 and was measured using the STJ array detector. The peak observed at 1250 eV is an Mg $K\alpha$ line, and the two peaks and a shoulder observed at 1100–1200 eV are Ga L lines. The Mg $K\alpha$ peak was separated from the adjacent Ga $L\beta_{3,4}$ peak, which was achieved by the high energy resolution of the detector. In this regard, the Mg $K\alpha$ peak was not separated from the Ga peak by a conventional SDD (detector: SiriusSD A30133LE-ISF-V, RaySpec Ltd) at the bending magnet beamline BL1N2 of the Aichi Synchrotron Radiation Center, Japan (Takeda, 2016), and was not detected even by WDX (analyzing crystal: thallium acid phthalate; detector: a gas-flow-type proportional counter, Rigaku Co.) at the undulator beamline BL16XU of the Super Photon Ring 8 GeV (SPring-8), Japan (Hirai *et al.*, 2004) (both data sets are not shown). The experimental Mg K-edge XANES spectrum is shown in Fig. 3. The edge of the XANES spectrum is ∼1307 eV, which is consistent with the report of Yonemura *et al.* (2013). Although the signal-to-noise ratio of the XANES spectrum is slightly lower, characteristic peaks can be seen at 1308, 1313 and 1324 eV (peaks I, II and III, respectively). However, the spectrum of the sample annealed at 800°C (the same temperature as ours) reported by Yonemura *et al.* shows clear peaks at 1309, 1312 and 1317 eV, which is different from the spectral feature shown in Fig. 3. We annealed the sample in an N_2 atmosphere but Yonemura *et al.* do not specify the atmosphere. If the sample was annealed in a vacuum, nitrogen desorption may occur, which can cause the atomic structure around Mg to differ.

The simulated Mg K-edge XANES spectra for Mg incorporated in GaN are shown in Fig. 4, with H around Mg. Among the six structures in which H was incorporated around

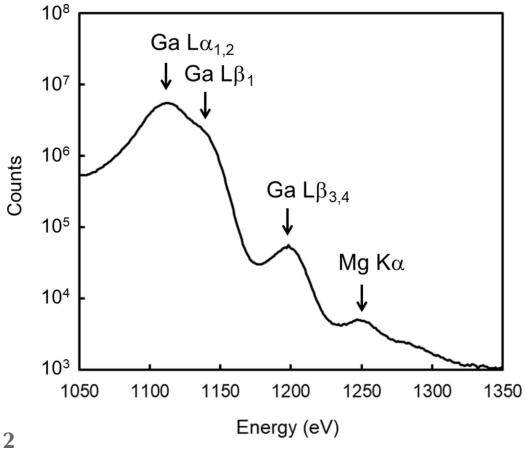

Figure 2
The X-ray fluorescence spectrum for Mg-doped GaN irradiated with X-rays of 1350 eV.

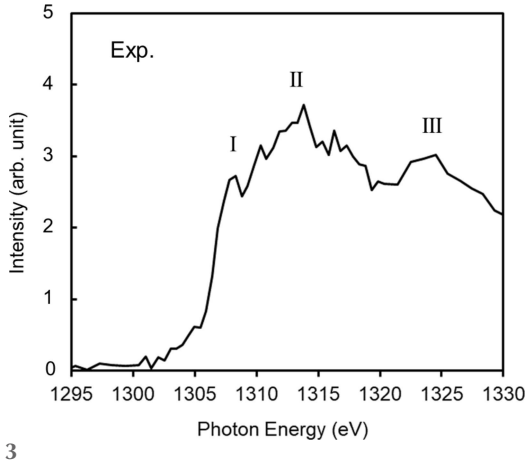

Figure 3
The measured Mg K-edge XANES spectrum for Mg-doped GaN. I, II and III indicate characteristic peaks.

Mg, the structure in which H was incorporated into the AB⊥ site (Mg–H[AB⊥]) was reported as the most stable by Park & Chang (2012) and is also the lowest energy in our calculations although within 0.3 eV. The structure in which H was incorporated into the BC‖ site is only ∼0.05 eV more than the most stable Mg–H[AB⊥] in our calculations (Table 1), and the spectrum for Mg–H[BC‖] is also shown in Fig. 4.

The structure in which Mg substitutes for the Ga site (Mg[Ga]) displays a spectrum with peaks at 1308, 1313 and 1323 eV, corresponding to the peaks I, II and III, respectively, as shown in Fig. 4. However, the structure in which Mg is incorporated into the interstitial site (Mg[interstitial]) displays

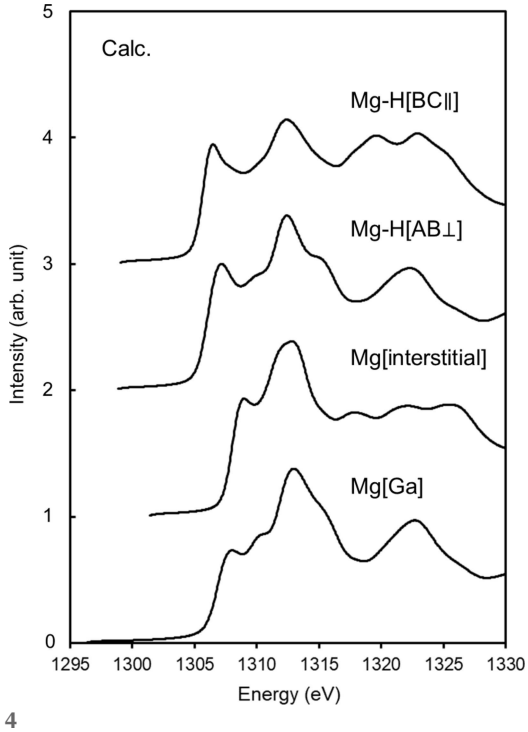

Figure 4
The simulated Mg K-edge XANES spectra for Mg incorporated into GaN, and with H. The brackets indicate Mg or H incorporated sites, which are shown in Fig. 1.

Table 1
Theoretically calculated energy differences for GaN with interstitial H, for the various lattice locations shown in Fig. 1.

Configuration	Energy (eV)
AB⊥	0.000
BC∥	0.052
AB∥	0.208
OA⊥	0.232
AB′∥	0.267
BC⊥	0.272

peak I with higher energy (∼1 eV) while peak III is not clearly observed, although the energy of peak II is the same as that for Mg[Ga]. The features (peak energies) of the measured spectrum (Fig. 3) almost agree with that of the simulated spectrum of Mg[Ga] and are mostly completely different from that of Mg[interstitial]. This suggests that Mg substitutes for the Ga site in the Mg-doped GaN sample. The Mg-doped GaN sample contained approximately the same amount of H as Mg before annealing, but the H decreased after annealing, which was confirmed by the H decreasing below the detection limit (10^{16} atoms cm^{-3}) of SIMS (Narita *et al.*, 2018). Hence, Mg–H complexes would probably be minimal and much of the Mg would substitute for Ga sites, which is consistent with the above-mentioned hypothesis (Mg could substitute for the Ga site).

In addition, the structures in which H atoms were incorporated around Mg (Mg–H[AB⊥] and Mg–H[BC∥]) indicated peak I with lower energy (1–1.5 eV) and higher intensity with respect to that of Mg[Ga], although the energy of peak II is the same as that for Mg[Ga], as shown in Fig. 4. Although phosphorus (P) *K*-edge XANES spectra simulated for P-incorporated diamond are expected as a wide bandgap semiconductor, the peak for the substitutional site with H around P occurs at ∼1 eV lower energy than that without H around P (Shikata *et al.*, 2020).

Thus, by comparing the measured spectrum with the simulated spectra in terms of spectral features such as edge and peak energies, the incorporated site of Mg can be investigated to determine that Mg doped in the GaN substitute for the Ga sites. In addition, not only the presence of H but also the incorporated site can be identified.

4. Conclusions

We have demonstrated local atomic structure analysis around Mg doped in GaN through XAS measurements using an STJ array detector and spectrum simulations using DFT. The XANES spectrum of Mg with 3×10^{19} atoms cm^{-3} was successfully obtained using the high sensitivity and high energy resolution of the detector. The incorporated site of Mg was identified as the Ga substitutional site by comparing the measured spectrum with the simulated spectra. In addition, the presence or absence of H around Mg can be identified with distinctive features in the simulated spectra. Hence, this combined experimental and theoretical XAS technique using the STJ array detector enables the local atomic structure analysis of Mg doped in GaN and, thus, contributes to the development of GaN power semiconductor devices.

Acknowledgements

Part of this work was supported by the AIST Nanocharacterization Facility (ANCF) as a program of 'Nanotechnology Platform' of the Ministry of Education, Culture, Sports, Science and Technology (MEXT) (Grant Number JPMXP09A19AT0005). We are grateful to Shigetomo Shiki and Tomoaki Ishizuka of AIST for XAS measurements. The synchrotron radiation measurements were performed at beamline BL-16A of the Photon Factory under the approval of the Photon Factory Program Advisory Committee (Proposal No. 2019L007). Auxiliary measurements were conducted at beamline BL1N2 of the Aichi Synchrotron Radiation Center, Aichi Science and Technology Foundation (Experiment No. 201901030), and at beamline BL16XU of SPring-8 with the approval of the Japan Synchrotron Radiation Research Institute (Proposal No. 2019A5070).

References

Amano, H., Kito, M., Hiramatsu, K. & Akasaki, I. (1989). *Jpn. J. Appl. Phys.* **28**, L2112–L2114.

Amemiya, K., Toyoshima, A., Kikuchi, T., Kosuge, T., Nigorikawa, K., Sumii, R., Ito, K., Garrett, R., Gentle, I., Nugent, K. & Wilkins, S. (2010). *AIP Conf. Proc.* **1234**, 295–298.

Bennett, S. E., Ulfig, R. M., Clifton, P. H., Kappers, M. J., Barnard, J. S., Humphreys, C. J. & Oliver, R. A. (2011). *Ultramicroscopy*, **111**, 207–211.

Clark, S. J., Segall, M. D., Pickard, C. J., Hasnip, P. J., Probert, M. I. J., Refson, K. & Payne, M. C. (2005). *Z. Kristallogr.* **220**, 567.

Gao, S.-P., Pickard, C. J., Perlov, A. & Milman, V. (2009). *J. Phys. Condens. Matter*, **21**, 104203.

Hirai, Y., Yasuami, S., Kobayashi, A., Hirai, Y., Nishino, J., Shibata, M., Yamaguchi, K., Liu, K.-Y., Kawado, S., Yamamoto, T., Noguchi, S., Takahashi, M., Konomi, I., Kimura, S., Hasegawa, M., Awaji, N., Komiya, S., Hirose, T., Ozaki, S., Okajima, T., Ishikawa, T. & Kitamura, H. (2004). *Nucl. Instrum. Methods Phys. Res. A*, **521**, 538–548.

Isomura, N., Kataoka, K., Watanabe, Y. & Kimoto, Y. (2019). *Jpn. J. Appl. Phys.* **58**, 051007.

Isomura, N., Kutsuki, K., Kataoka, K., Watanabe, Y. & Kimoto, Y. (2019). *J. Synchrotron Rad.* **26**, 462–466.

Isomura, N., Nagaoka, T., Watanabe, Y., Kutsuki, K., Nishinaka, H. & Yoshimoto, M. (2020). *Jpn. J. Appl. Phys.*. **59**, 070909.

Kachi, T. (2014). *Jpn. J. Appl. Phys.* **53**, 100210.

Kanechika, M., Sugimoto, M., Soejima, N., Ueda, H., Ishiguro, O., Kodama, M., Hayashi, E., Itoh, K., Uesugi, T. & Kachi, T. (2007). *Jpn. J. Appl. Phys.* **46**, L503–L505.

Mizoguchi, T., Matsunaga, K., Tochigi, E. & Ikuhara, Y. (2012). *Micron*, **43**, 37–42.

Mizoguchi, T., Tanaka, I., Gao, S.-P. & Pickard, C. J. (2009). *J. Phys. Condens. Matter*, **21**, 104204.

Nakamura, S., Iwasa, N., Senoh, M. & Mukai, T. (1992). *Jpn. J. Appl. Phys.* **31**, 1258–1266.

Narita, T., Kachi, T., Kataoka, K. & Uesugi, T. (2017). *Appl. Phys. Expr.* **10**, 016501.

Narita, T., Tokuda, Y., Kogiso, T., Tomita, K. & Kachi, T. (2018). *J. Appl. Phys.* **123**, 161405.

Neugebauer, J. & Van de Walle, C. G. (1999). *J. Appl. Phys.* **85**, 3003–3005.
Norman, D. (1986). *J. Phys. C. Solid State Phys.* **19**, 3273–3311.
Ohkubo, M., Shiki, S., Ukibe, M., Matsubayashi, N., Kitajima, Y. & Nagamachi, S. (2012). *Sci. Rep.* **2**, 831.
Park, J.-S. & Chang, K. J. (2012). *Appl. Phys. Expr.* **5**, 065601.
Perdew, J. P., Burke, K. & Ernzerhof, M. (1996). *Phys. Rev. Lett.* **77**, 3865–3868.
Shikata, S., Yamaguchi, K., Fujiwara, A., Tamenori, Y., Tsuruta, K., Yamada, T., Nicley, S. S., Haenen, K. & Koizumi, S. (2020). *Diamond Relat. Mater.* **105**, 107769.
Shiki, S., Ukibe, M., Matsubayashi, N., Zen, N., Koike, M., Kitajima, Y. & Ohkubo, M. (2014). *J. Low Temp. Phys.* **176**, 604–609.
Takeda, Y. (2016). *J. Phys. Conf. Ser.* **712**, 012146.
Yonemura, T., Iihara, J., Saito, Y. & Ueno, M. (2013). *Jpn. J. Appl. Phys.* **52**, 126602.